Catalysis Today xxx (2016) xxx–xxx

Contents lists available at ScienceDirect

Catalysis Today

journal homepage: www.elsevier.com/locate/cattod

Influence of acidic properties of different solid acid catalysts for glycerol acetylation

B.O. Dalla Costa [a], H.P. Decolatti [a], M.S. Legnoverde [b], C.A. Querini [a,*]

[a] Instituto de Investigaciones en Catálisis y Petroquímica (INCAPE) – FIQ – UNL – CONICET, Santiago del Estero 2654, Santa Fe, S3000AOJ, Argentina
[b] Centro de Investigación y Desarrollo en Ciencias Aplicadas (CINDECA) – FCE – UNLP – CONICET, Calle 47 N° 257, La Plata, B1900AJK, Argentina

ARTICLE INFO

Article history:
Received 20 May 2016
Received in revised form 23 August 2016
Accepted 9 September 2016
Available online xxx

Keywords:
Mesoporous silica
Glycerol acetylation
HZSM5
Beta zeolite

ABSTRACT

The glycerol esterification with acetic acid is studied in this work using propylsulfonic functionalized mesoporous silica (Pr-SO_3H-SBA-15), and compared with H-ZSM-5 and H-Beta zeolites. The reaction was carried out in a batch reactor using a 6:1 molar ratio of acetic acid to glycerol. The initial TOF for the glycerol conversion was significantly higher in the propylsulfonic mesoporous silica, as compared to the two zeolites. These two catalysts have acid sites densities (μmol m^{-2}) that are less than half than that displayed by the SBA-based catalyst. It was possible to obtain 96% conversion in 2.5 h, with 87% selectivity to the products of interest diacetylglycerol (DAG) + triacetylglycerol (TAG), being the ratio DAG/TAG = 1.7. The catalyst deactivates partly due to sulfonic groups loss and to coke deposition during the reaction, as observed when it was used in a second reaction cycle without any treatment in between cycles. The catalyst lost activity, but maintained the selectivity, associated to a non-selective site poisoning.

1. Introduction

Glycerol is a polyol obtained as a by-product during the synthesis of biodiesel by transesterification of triglycerides with methanol or ethanol. The increase in the biodiesel production in recent years has led to an accumulation of glycerol in the global market. Because of this, the price of glycerol has dropped dramatically, and numerous researches to find new applications and processes to obtain products of higher value added have been proposed.

Acetylation of glycerol by esterification with acetic acid has been studied as an interesting alternative, to obtain monoacetin (monoacetylglycerol MAG), diacetin (DAG) and triacetin (TAG) as products [1–7]. DAG and TAG are the more valuable compounds due to their wide applications as fuel additives and solvents [8–11]. Adding a small amount of TAG into biodiesel improves its viscosity and low-temperature properties. The decrease in the cloud point (CP) and pour point (PP) of biodiesel is due to the low freezing point of triacetin, while the higher viscosity of triacetin prevents a decrease of the cold filter plugging point (CFPP) [12].

One of the challenges in this reaction system is the separation of compounds, because they have similar boiling points [1,3,13,14]. Another drawback is the low selectivity towards the more important product (TAG), due to the formation of water and acetol by-products which negatively affects the thermodynamic equilibrium [15]. One way to improve the selectivity to TAG is using acetic anhydride as acetylating agent [17], or making two acetylation steps, first with acetic acid and then with acetic anhydride [15,16]. However, the disadvantage of this procedure is the price of the acetylating agent. Another alternative to effectively shift the chemical equilibrium is to use toluene to continuously remove the reaction water [18].

The glycerol acetylation reaction proceeds by an acid-catalyzed mechanism. Homogeneous catalysts can be employed. The disadvantages are the corrosion caused in the reactors, the production of toxic compounds, and the loss of catalysts due to the difficulty of their separation. For these reasons, different solid catalysts like commercial resins Amberlyst-15 and zeolites have been studied in order to substitute the liquids [1,19,20]. Kim et al. [21] reported studies with different catalysts, such as propyl sulfonic acid functionalized SBA-15 (Pr-SO_3H-SBA-15), sulfonic acid functionalized SBA-15 (SO_3H-SBA-15), and microcrystalline cellulose catalysts. Magnetic solid acid catalysts were also evaluated in this reaction [22]. Results obtained with the H-BETA zeolite (SiO_2/Al_2O_3 = 25) was reported by Sandesh et al. [23], while an H-ZSM-5 (Si/Al = 28) was previously used in this reaction [1].

SBA-15 materials containing sulfonic groups on its surface were tested in different esterification reactions, such as the esterification of free fatty acids with methanol [24–27]. The activity of these

* Corresponding author at: Santiago del Estero 2654-(3000), Santa Fe, Argentina.
E-mail address: querini@fiq.unl.edu.ar (C.A. Querini)

http://dx.doi.org/10.1016/j.cattod.2016.09.015
0920-5861/

materials for these reactions suggests the presence of strong acid sites. Moreover, it was found that the structure and the acid sites nature of Pr-SO_3H-SBA-15 catalyst were responsible for the catalytic performance in the direct esterification of acrylic acid with cyclohexene [28]. These catalysts were also employed in the acetylation of glycerol [21,29,30]. It is important to highlight that the Pr-SO_3H-SBA-15 catalysts used in these three publications, have lower acid sites density than the catalyst used in the present study, as discussed below.

Comparative studies of several catalysts under identical reaction conditions are necessary in order to investigate the effect of surface acidity (amount and strength of acid sites) and the porous structure. In this work two microporous zeolites, H-ZSM-5 (Si/Al = 15) and H-Beta (Si/Al = 13), with a similar density but different strength of acid sites are studied. Furthermore, a mesoporous silica SBA-15 with propyl-sulfonic functional groups (Pr-SO_3H-SBA-15) is also evaluated. The activity and selectivity results are correlated with the acidic and textural properties, which were determined using several characterization techniques.

2. Experimental

2.1. Catalysts synthesis

The propyl-mercapto mesoporous silica (Pr-SH-SBA-15) material was synthesized by co-condensation of Tetraethylorthosilicate (TEOS, 98%, Aldrich) and Mercaptopropyltrimethoxysilane (MPTMS, 95%, Aldrich), in the presence of a copolymer poly(ethyleneglycol)-block-poly(propyleneglycol)-block-poly (ethyleneglycol) (PE-PP-PE Pluronic P123, Aldrich) as the structure-directing agent, and in HCl (Baker) acid medium, employing the sol-gel technique. The molar composition of each mixture for 4 g of copolymer was 0.0369TEOS:0.0041MPTMS:0.24HCl:6.67H_2O. The resultant solution was stirred for 20 h at 40 °C, after which the mixture was aged at 80 °C for 70 h under static conditions. Then, the solid product was recovered by filtration and dried in air at room-temperature overnight. To remove the template from the as-synthesized material, it was washed with ethanol under reflux for 24 h, using 100 ml of ethanol per gram of material. After thiol functionalization, the oxidation was made according to the method described by Bossaert et al. [31] by soaking the resulting solid in an aqueous dissolution of hydrogen peroxide (H_2O_2 30 vol%, Panreac). After the oxidation step, the solution was filtered and the solid was washed with ethanol. The wet solid was suspended (1 wt%) in 1 M H_2SO_4 solution for 2 h. The powder was then washed with water and ethanol and dried for 2 h at 120 °C. This catalyst was labeled Pr-SO_3H-SBA-15.

Furthermore, a mesoporous silica SBA-15 without functional groups was synthesized employing the procedure described by Zhao et al. [32]. In the preparation, 4 g of Pluronic P123 block copolymer were dissolved in an aqueous solution of HCl (2 mol L^{-1}) and stirring at 35 °C. Then, TEOS was added drop by drop while stirring for 20 h. The mixture was then heated to 80 °C for 24 h. In this case, the molar composition used was 1TEOS:5HCl:0.018PEO:184H_2O. Finally, the solid material obtained was washed with water, dried at 120 °C and calcined for 6 h at 540 °C.

Commercial H-ZSM-5 (CBV-3020E, Si/Al = 15) and H-Beta (UOP, Si/Al = 13) zeolites were also used in this study.

2.2. Catalysts characterization

Nitrogen adsorption-desorption isotherms were recorded at the temperature of liquid nitrogen (−196 °C) in a Micrometrics ASAP 2020 instrument. Before adsorption, samples were evacuated by heating at 100 °C or at 250 °C for the Pr-SO_3H-SBA-15 and for zeolites respectively, in vacuum, with a pressure lower than 4×10^{-2} mbar during 12 h. The lower temperature of treatment for the mesoporous material was selected according to the thermal stability of the functional groups. The surface was calculated according to the Brunauer–Emmett–Teller (BET) equation, in the relative pressure range 0.01–0.10 [33]. The micropore volume and external area in zeolites was derived from the t-plot, according to Lippens and de Boer [34]. The pore size distribution in the mesoporous materials was obtained by the BJH method [35].

The XPS analyses were carried out employing a multi-technique system (SPECS) equipped with a dual Mg/Al X-ray source and a hemi-spherical PHOIBOS 150 analyzer operating in the fixed analyzer transmission (FAT) mode. The spectra were obtained with pass energy of 30 eV and the Mg anode was operated at 200 W, measuring the core level signals of O 1s, Si 2p, S 2p and C 1 s and with a multi-channel detector. The working pressure in the analyzing chamber was lower than 2 10^{-8} mbar. The samples were mounted on a sample rod, placed in the pre-treatment chamber of the spectrometer, submitted to evacuation for 10 min at 120 °C, and then evacuated at ultra high vacuum for 2 h. The software CasaXPS (Casa Software Ltd, UK) was used to process the spectra. For the estimation of the intensities the integral of each peak was calculated after subtracting a Shirley-type background and fitting the experimental curve to a combination of Lorentzian and Gaussian lines. The C1 peak (284.6 eV) was used as reference to the binding energy values. Sensitivity factors provided by the manufacturers were employed for the quantification of the elements.

FT-IR spectra of samples SBA-15 and Pr-SO_3H-SBA-15 were collected in an FT-IR Spectrometer Spectrum 1000, Perkin Elmer, employing KBr in the frequency range of 4000–400 cm^{-1}.

Scanning electron microscopy (SEM) was carried out on Philips 505 microscope. For preparation of samples, a small amount of sample was placed on carbon tape and sputter coated with gold.

The amount and strength of acid sites in the zeolites was evaluated by Pyridine Temperature- programmed desorption (TPD). Approximately 10 mg of catalysts, sandwiched by quartz wool, was loaded in a quartz tube. The catalysts were pretreated in-situ in N_2 flow (30 ml min^{-1}) at 350 °C for 1 h. After cooling down to room temperature, the sample was saturated with pyridine. Then, pure nitrogen was flowed and the temperature was increased up to 150 °C, maintaining this temperature until no physically adsorbed pyridine was detected. The TPD experiment was carried out heating at 12 °C min^{-1} in nitrogen flow from 150 °C to 750 °C. Pyridine coming out of the sample cell passed through a methanation reactor. To this reactor a H_2 stream was also fed, quantitatively converting Pyridine to CH_4, using a Ni catalyst. The CH_4 was continuously measured by a FID detector.

The change in acidity due to functionalization in the Pr-SO_3H-SBA-15 catalyst was determined by potentiometric titration, because the decomposition of the functional groups interferes with the determination by pyridine TPD. A known mass of the solid to be analyzed was suspended in acetonitrile. The suspension was titrated using a solution of *n*-butylamine in acetonitrile (0.1 mol L^{-1}) at 0.05 ml min^{-1}. The electrode potential variation was obtained on a digital pH meter (Metrohm 794 Basic Titrino apparatus with a double junction electrode).

The electrical potential of the catalysts dissolved in acetonitrile was determined for the three catalysts used in the present study. This value is indicative of the strength of the acid sites.

The thermal stability of the Pr-SO_3H-SBA-15 catalyst was studied by thermogravimetry (TGA), in a Netzsch STA 449F3 instrument. Approximately 5 mg of sample was loaded into an alumina crucible and heated at 10 °C min^{-1}, from 20 °C to 700 °C, with a N_2 flow rate of 50 ml min^{-1}. The differential thermal gravimetric profiles (DTG) were obtained from the TGA profiles.

Please cite this article in press as: B.O. Dalla Costa, et al., Influence of acidic properties of different solid acid catalysts for glycerol acetylation, Catal. Today (2016), http://dx.doi.org/10.1016/j.cattod.2016.09.015

Also the temperature-programmed desorption equipment was used to perform a thermal stability test. These experiments were carried out in the same equipment described before for the Pyridine TPD experiments, but without adsorbing any probe molecule. The decomposition of the propyl sulfonic chains and its subsequent methanation allowed the detection by FID.

The sulfur content in the catalyst Pr-SO_3H-SBA-15 before and after reaction was measured by Energy-dispersive X-ray fluorescence (XRF), using a Shimadzu equipment, model EDX-720, working in the energy dispersion mode.

2.3. Catalyst performance tests

Glycerol acetylation reaction was carried out in a stirred batch reactor at 120 °C and atmospheric pressure. The reactants used were acetic acid (Anedra, Glacial 99.8%) and glycerol (Biopack 99.5%) with a molar ratio 6:1. The zeolites and Pr-SO_3H-SBA-15 catalysts were dried at 300 °C and 200 °C respectively for 12 h prior to reaction. The lower temperature of drying for the mesoporous material was selected in order to eliminate water but preserving the functional groups, which decompose above the 300 °C according thermal stability studies. The glycerol containing 4 wt% of catalyst (relative to glycerol), was heated to the reaction temperature, and then the acetic acid was injected to the system. Sampling of the product mixture was made every 30 min, and the composition was analyzed by gas chromatography (Agilent 7820A, HP-FFAP column (30 m × 0.32 mm × 0.25 μm)) equipped with a flame ionization detector (FID). To verify the calibration and analyses, the concentration of glycerol in the collected samples was also determined by a volumetric method [36].

The glycerol conversion and the selectivities of each product were calculated as follows:

$$\text{Glycerol conversion}\,(\%) = \frac{\text{amount of converted glycerol}}{\text{total amount of fed glycerol}} \times 100$$

$$\text{Selectivity}\,(\%) = \frac{\text{amount of glycerol converted to a product}}{\text{total amount of converted glycerol}} \times 100$$

2.3.1. Catalyst reuse

A single experiment was carried out with the Pr-SO_3H-SBA-15 catalyst, using the same catalyst sample in two consecutive cycles. The catalyst was reused without any treatment, after filtration from the reaction media of the first cycle.

3. Results and discussion

3.1. Catalysts characterization

3.1.1. Textural properties

The N_2 adsorption–desorption isotherms for the Pr-SO_3H-SBA-15 and SBA-15 materials are shown in Fig. 1A. In both cases, type IV isotherms characteristic of mesoporous structures were observed, with a H1 hysteresis loop, which is associated to capillary condensation in the mesopores [37]. The relationship between the adsorption increase at $P/P_0 < 0.4$ corresponding to the multilayer adsorption and the second increase at $P/P_0 = 0.4–0.7$, depends on the presence of functional groups. Furthermore, the hysteresis loop suffers changes after functionalization. The capillary condensation step for the functionalized sample Pr-SO_3H-SBA-15 is closing down at P/P_0 equal to 0.40, a lower value in comparison to 0.45 for the original SBA-15, indicating that the pores suffer narrowing after functionalization.

The mesopores size distributions (Fig. 1B) were calculated using the thermodynamic-based Barret-Joyner-Halenda (BJH) method, using the desorption branch of the isotherm for the SBA-15. Instead, for the sample Pr-SO_3H-SBA-15 the adsorption branch was used to evaluate the pore size distribution. The reason is the cavitation phenomenon that can be present in this sample, because the hysteresis loop for the nitrogen isotherms is closing near to 0.40–0.42 in relative pressure [38,39].

The textural characteristics of all studied materials are summarized in Table 1. In the functionalized sample it can be noticed an important decrease of the surface and pore volume, in comparison with the SBA-15. Other possible cause of the decrease of the pore volume in the functionalized sample could be due to the presence of template, which can not be completely removed by washing with ethanol. This is achieved most effectively by calcining the SBA-15 sample. Due to problems of thermal stability of the functional groups at temperatures above 300 °C (as shown below in DTG and TPD results), the washing with ethanol is adopted in sample Pr-SO_3H-SBA-15. In view of the results, it is assumed that during the outgassing at 100 °C under vacuum prior to the N_2 adsorption–desorption measurements, not all the template is removed in the Pr-SO_3H-SBA-15 sample.

As mentioned before, the co-condensation method was selected for the synthesis of the Pr-SO_3H-SBA-15, in order to obtain a high loading density with a homogeneous distribution of the functional groups, despite knowing that by this method the extraction efficiency for the block copolymer systems were only ca. 80% [40]. By XPS analyses it is possible to estimate the amount of template left in the catalyst, as discussed bellow. However, differences in the textural properties cannot be associated only to the presence of template residues within the pores.

The N_2 adsorption-desorption isotherms obtained for the zeolites H-Beta and H-ZSM-5 (Fig. 1A) were characteristic of microporous materials. Both zeolites exhibit a type I isotherm with a plateau at high relative pressures, as a result of the microporous nature of the material with limited mesoporosity. Besides, a type H4 hysteresis was observed, and since these zeolites displayed a type I isotherm, this hysteresis is also a sign of microporosity.

The H-ZSM-5 zeolite has a two dimensional channel structure (linked by much smaller channels), with pore diameter of 5.6 Å. The BET surface for this material was similar to the H-Beta, while the latter has a greater micropore volume. The reason is the three dimensional structure in this zeolite, with cages of 7 Å.

SEM images (Fig. 2A) reveal the typical form of SBA-15 particles as agglomerates with the form of wheat grains composed of small cylinders. SEM micrographs indicate that the presence of MPTS in the synthesis media do not alter the usual morphology presented by SBA-15 structure, but the size of these agglomerates is smaller in the functionalized sample (Fig. 2B). This can be explained considering that the morphologies depend on the evolution of the micelle shapes as a consequence of the interaction with the silicate [41], and MPTS interferes with this interaction.

3.1.2. XPS analysis

Table 2 resumes the surface chemical compositions of the Pr-SO_3H-SBA-15 and SBA-15 samples determined by XPS. The unfunctionalized support contains mainly silicon and oxygen on its surface. The carbon detected (1.65%) may correspond to residues of the template used during the synthesis, but it is low enough to indicate the effectiveness of the copolymer removal by calcination. As expected, the %C was increased due to the presence of propyl groups in the sample Pr-SO_3H-SBA-15, which proves the surface functionalization. Also sulfur was detected on its surface.

With the results of XPS in the functionalized sample an estimation of the content of template can be performed. Considering for each Pr-SO_3H- group attached to the surface an atomic ratio C/S = 3, knowing the sulfur content is possible to calculate the %C associated with those functional groups. Then, the difference with the

Please cite this article in press as: B.O. Dalla Costa, et al., Influence of acidic properties of different solid acid catalysts for glycerol acetylation, Catal. Today (2016), http://dx.doi.org/10.1016/j.cattod.2016.09.015

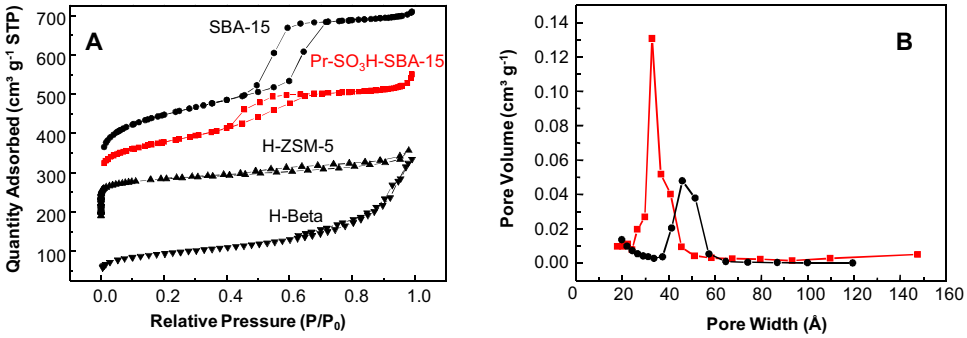

Fig. 1. (A) N_2 adsorption-desorption isotherms, (B) Pore size distribution; for samples SBA-15 (●), Pr-SO_3H-SBA-15 (■).

Table 1
Textural and acidic properties.

Sample	BET surface ($m^2\ g^{-1}$)	Mesop. surface ($m^2\ g^{-1}$)	Pore Vol ($cm^3\ g^{-1}$)	Pore size (Å)	Acidity (mmol g^{-1})	Acid site density (μmol m^{-2})
SBA-15	750	–	0.720	48	–	–
Pr-SO_3H-SBA-15	366	–	0.410	32	1.80	4.9
H-ZSM-5	570	255	0.136	5.6	0.97	1.7
H-Beta	588	210	0.191	5.6–7	1.08	1.9

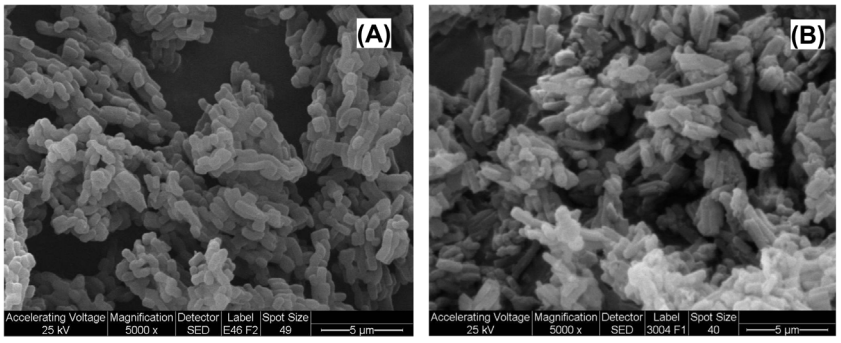

Fig. 2. SEM images: (A) SBA-15, (B) Pr-SO_3H-SBA-15.

Table 2
Surface chemical composition (atomic concentration %) obtained by XPS.

Sample	%C	%O	%Si	%S	$\%S_{merc}$	$\%S_{sulf}$
SBA-15	1.65	65.41	32.94	–		
Pr-SO_3H-SBA-15	11.50	58.00	25.80	4.7	9.0	91.0

%Smerc and %Ssulf corresponds to sulfur associated to propyl-SH and propyl-SO_3H groups respectively.

total %C corresponds to residues from the template. In this way, in the sample Pr-SO_3H-SBA-15 a residue of 6.2 %C was estimated.

It is possible also to determine with this technique, the degree of oxidation achieved in the functionalized sample, taking into account the XPS signals for sulfur. The XPS spectra of the S 2*p* signal corresponding to the Pr-SO_3H-SBA-15 catalyst have shown the presence of two oxidation states of sulfur (S^{6+} and S^{2-}), ascribed to the simultaneous presence of sulfonic (S 2*p*3/2 at 169.0 eV) and mercapto (S 2*p*3/2 at 163.8 eV) groups [42]. According to the results showed in Table 2, the 91% of the functional groups were effectively oxidized during the preparation of the sample.

3.1.3. FTIR analysis

The functionalization of SBA-15 silica can be followed also by FTIR. Fig. 3 shows the spectra corresponding to the original sample SBA-15 and after functionalization. The signals characteristic of the silica are present. The peak around 960 cm^{-1} corresponds to

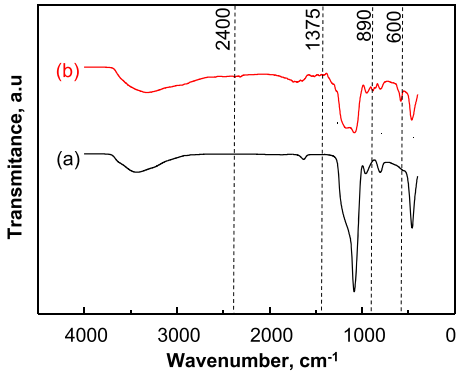

Fig. 3. FTIR spectra: (a) SBA-15, (b) Pr-SO_3H-SBA-15.

Please cite this article in press as: B.O. Dalla Costa, et al., Influence of acidic properties of different solid acid catalysts for glycerol acetylation, Catal. Today (2016), http://dx.doi.org/10.1016/j.cattod.2016.09.015

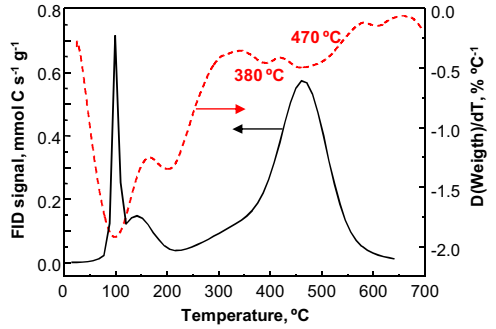

Fig. 4. TPD (solid line) and DTG (dashed line) for sample Pr-SO_3H-SBA-15.

non-condensed Si–OH groups [43,44]. Then, asymmetric stretching vibrations of Si–O–Si at 1100 cm^{-1}, symmetric stretching vibrations from Si–O bonds at 800 cm^{-1} and bending vibrations from Si–O–Si at 466 cm^{-1} are clearly observed. The stretching and bending vibrations of adsorbed H_2O are represented by the broad band around 3400 cm^{-1} and the peak around 1630 cm^{-1}.

In the Pr-SO_3H-SBA-15, the C—O—C vibrations at 1375 cm^{-1} evidence the presence of rest of copolymer. The signal is small but clearly different respect to the SBA-15 spectra, and indicates that there is a new signal at this wavenumber. Moreover, the bands at 600 and 890 cm^{-1} are due to C—S and S—O stretching vibrations, respectively [45]. The vibration corresponding to the SH group was not observed at 2600 cm^{-1} [46], indicating that the presence of non-oxidized groups was no detected by this technique. There is a weak signal at 2400 cm^{-1}. It is known that at 2400 cm^{-1} the C—O bond in CO_2 presents the signal that corresponds to the symmetric and asymmetric stretching. However, the non-functionalized SBA did not show the signal at this wavenumber, and besides the catalysts were pre-evacuated before the FTIR analysis. Therefore, it is not clear to which group this signal belongs to.

3.1.4. Thermal stability

To study the thermal stability of the Pr-SO_3H-SBA-15 catalyst, TGA and TPD experiments were employed. Many authors attributed to the loss of physisorbed water in the material the decrease in weight around 100 °C observed in the DTG profile (Fig. 4 dashed line) [47]. Also, a maximum in the signal at 100 °C was observed in the TPD experiment (Fig. 4, solid line). However, the FID detector used in this technique is not responsive to water. Therefore, this decrease in weight is necessarily associated also with carbon molecules that are desorbed from the surface during the heating in nitrogen flow. These are moieties of the block copolymer that were previously observed by XPS and that were not efficiently removed in the washing steps during the catalyst synthesis. Besides, it is also possible that if water is removed during heating, this helps the release of these compounds.

Going to higher temperatures in the DTG profile, two peaks with maxima at 380 °C and 470 °C can be observed, indicating the decomposition of propyl-SH and propyl-SO_3 groups respectively [48]. Note that the size of the peak at 470 °C in the TPD profile is larger than in the DTG curve, and this is due to the high sensitivity of the FID detector for carbonaceous compounds analysis.

The shoulder displayed around 360–400 °C in the TPD profile corresponds to the decomposition of propyl-SH groups, as previously suggested by other authors [48,49] using DTG analyses. It must be mentioned that both types of experiments (TPD and DTG) were carried out using the same carrier gas and similar heating rates. The presence of these non-oxidized groups was not clearly visible in the IR spectrum of the sample (Fig. 3, curve b). In addition, in the XPS spectra their signal was much lower than the corresponding to sulfonic groups (not shown). According to these results, the sample Pr-SO_3H-SBA-15 has mainly oxidized sites (sulfonic groups), with good thermal stability, better than that reported by other authors. Finally, the loss of functional groups from 300 °C in N_2 stream can not be completely ruled out due to the increase in the FID signal in the TPD profile. For this reason, treatment prior to the reaction was performed at only 200 °C.

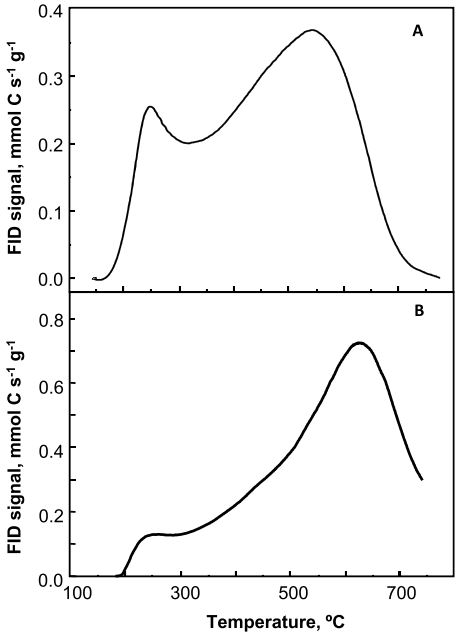

Fig. 5. Pyridine TPD profiles for the zeolites H-Beta (A) and H-ZSM-5 (B).

3.1.5. Acidity

Fig. 5 shows the Pyridine TPD profiles for the zeolites, and Table 1 shows the acid sites quantification. The H-Beta and H-ZSM-5 catalysts present similar content of adsorbed pyridine, indicating that the amount of acid sites is comparable for these catalysts. These results correlate with the Si/Al ratio in these materials. The capacity of pyridine adsorption observed in the H-Beta zeolite was 1.08 mmol g^{-1}, which is close to the theoretical concentration of Al sites (1.05 mmol g^{-1}), corresponding to the ratio Si/Al = 13. Sandesh et al. [23] studied a similar H-Beta catalyst (SiO_2/Al_2O_3 = 25, S_{BET} = 450 m^2 g^{-1}) detecting 1.48 mmol g^{-1} of acid sites by potentiometric acid-base titration with *n*-butylamine.

The H-ZSM-5 showed an amount of acid sites detected by pyridine adsorption of 0.97 mmol g^{-1}, lower than that observed for the H-Beta. However, considering the BET areas, the density of acid sites for these materials were practically the same. Gonçalves et al., [1] studied glycerol acetylation with different solid acids, including an H-ZSM-5 with: Si/Al = 28, S_{BET} = 374 m^2 g^{-1} and acidity = 1.2 mmol g^{-1}.

While similar pyridine adsorption capacities were quantified on the studied zeolites, significant differences were observed respect to the strength of the acid sites, according to the temperature desorption of pyridine. In the case of the H-Beta catalyst, the profile displays two peaks at 250 °C and 550 °C corresponding to acid sites of weak/medium and strong acidity respectively. The amount of each type of acid site was comparable in this material. In the case of the H-ZSM-5 zeolite instead, sites of weak/medium strength are also observed with a peak desorption at 250 °C, but in a lower amount than in the case of sites of high strength, associated with the peak at 620 °C. Furthermore, it must be noted that temperatures above 750 °C were required to completely desorb the pyridine

Please cite this article in press as: B.O. Dalla Costa, et al., Influence of acidic properties of different solid acid catalysts for glycerol acetylation, Catal. Today (2016), http://dx.doi.org/10.1016/j.cattod.2016.09.015

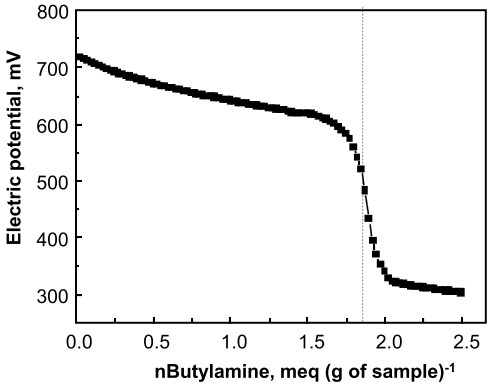

Fig. 6. Potentiometric titration with *n*-butylamine of sample Pr-SO_3H-SBA-15.

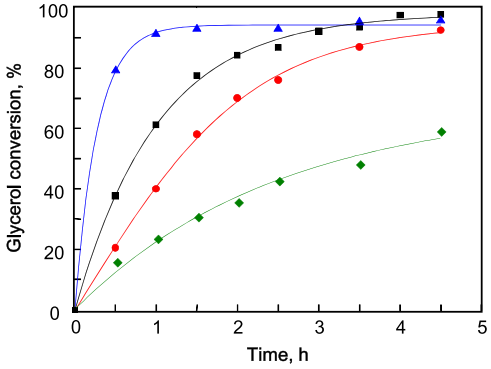

Fig. 7. Glycerol conversion as a function of reaction time for samples Pr-SO_3H-SBA-15 (▲), H-ZSM-5 (■),H-Beta (●) and blank test (♦).

from this catalyst, thus indicating the significant strength of the acid sites.

In the case of the mesoporous material Pr-SO_3H-SBA-15, the acidity was determined by potentiometric titration with *n*-butylamine. This technique was used because the pyridine TPD is inappropriate, since the FID detector is sensitive to both the pyridine and the propyl groups that decompose during heating. Fig. 6 shows the potentiometric titration curve of the functionalized sample. In the case of the non-functionalized SBA-15 support, no acidity was detected, as previously reported [24]. A higher value of initial potential in the titration curve of the sample indicates an appreciable strength of the sulfonic acid groups. A total amount of acid sites of 1.8 mmol g^{-1} was detected for this sample, as determined by the inflection point of the curve. Contrary to what happens for zeolites, for this material all the active sites have the same acid strength and accessibility. The Pr-SO_3H-SBA-15 catalysts studied by other authors showed acidities around 1.2 mmol g^{-1}, in addition with higher BET areas (around 500–700 m^2 g^{-1}) [21,29,30], which resulted in acid site densities of 1.2 μmol m^{-2} [21], 3.1 μmol m^{-2} [29], and 1.7 μmol m^{-2} [30]. These values are lower than that presented by the Pr-SO_3H-SBA-15 catalyst synthesized in this work, which has an acid sites density of 4.92 μmol m^{-2}. In addition, this value is practically the double than that of zeolites. The textural and acidity results for the three materials are summarized in Table 1.

3.1.6. Activity results

Fig. 7 shows the glycerol conversion during the acetylation reaction, for the three studied materials and the experiment without solid catalyst (blank test). In all cases an improvement of the reaction rate was achieved using solid acid catalysts. It is important to emphasize that the esterification reaction is catalyzed by acids, and one of the reactants is the acetic acid, and therefore the reaction proceeds at an appreciable rate even in the absence of other catalyst, although as observed in Fig. 7, at a much lower rate. A high reaction rate is observed at the beginning of the reaction with the Pr-SO_3H-SBA-15 catalyst, reaching the final value of 96% in less than two hours. For the zeolites instead, reaction times longer than 4 h are necessary to achieve the equilibrium conversion. Therefore, there is a direct correlation between total conversion and total acidity, behavior also observed by other authors who have studied various acidity levels for a same support [50], or various catalysts with different acid sites concentrations [29]. Thus, the mesoporous catalyst with higher acid site density was the more active among the materials studied in this work.

To analyze the effect of the strength of sites, results obtained for the zeolites are compared, taking into account that both zeolites have similar acid site density. According to the Pyridine TPD results the H-ZSM-5 possess more strong acid sites. This makes this solid more active in comparison to the H-Beta zeolite. At 2.5 h of reaction, the glycerol conversion was 87% for the H-ZSM-5 and 75% for H-Beta. This correlation between the enhancement in the acid strength on solid acids and the improvement in the activity was found by other authors, always comparing analogous catalysts [21], like in this case for the two zeolites. If sufficient reaction time for the zeolites is left, the equilibrium conversion appears to be slightly higher for the H-ZSM-5 catalyst, being even greater than that for the mesoporous solid. The final conversion seems to be different between H-ZSM-5 and Pr-SO_3H-SBA-15 catalysts. This could be due to an equilibrium shift caused by water adsorption in the case of the zeolite, while the surface of the Pr-SO_3H-SBA-15 catalyst is hydrophobic.

The selectivities as a function of reaction time for the three catalysts are shown in Fig. 8. On these materials, monoacetin (MAG), diacetin (DAG) and triacetin (TAG) were detected as reaction products, not observing other hydrocarbons unlike other authors [1,51]. The other reaction product was water. The Scheme 1 shows the reactions and products involved in the glycerol acetylation.

In all cases, at low reaction times the predominant product was MAG, which subsequently undergoes acetylation to DAG and to TAG finally. This is because from the thermodynamic point of view for these reactions, the Gibbís free energy of formation of 1-monoacetin (19.2 kJ mol^{-1}) is much lower than that of 1,3-diacetin (37.0 kJ mol^{-1}) and triacetin (92.5 kJ mol^{-1}) [52]. The product distribution obtained throughout the reaction time is typical of consecutive reactions limited by thermodynamic equilibrium, being the intermediate product in this case the DAG. The final composition reached depends on the activity of the solid and its capacity to expand to a greater degree the acetylation of the glycerol molecule. The Pr-SO_3H-SBA-15 catalyst was the most active, with a rapid conversion of glycerol at low reaction times. For this material, at 2.5 h the glycerol conversion was 96% and the product distribution was DAG (55%), TAG (32%) and MAG (13%). Because both are products of interest as valuable biodiesel and petro fuel additives [53–55], and also because its application does not require their separation, it is important to note that the global selectivity to (DAG + TAG) was 87% for this catalyst, which is really high. The TAG selectivity is higher than that obtained for a similar catalyst by Kim et al. [21], at longer reaction time (8 h) and higher catalyst loading (5 wt%) but at 80 °C. Testa et al. [29] achieved better results, reaching a selectivity to (DAG + TAG) equal to 95% after 3 h reaction at 105 °C, employing a ratio acetic acid to glycerol 3:1, loading 5 wt% of a catalyst propyl-sulfonic SBA-15 with an acidity of 1.54 mmol g^{-1}. The authors found a maximum in the TAG yield as a function of the catalyst surface acidic density close to 3 μmol m^{-2}, whereas in the present work the catalyst density is 4.9 μmol m^{-2}. The authors associated this behavior to the presence of steric hindrance when the spacing between the acidic groups is not enough to allow the

Please cite this article in press as: B.O. Dalla Costa, et al., Influence of acidic properties of different solid acid catalysts for glycerol acetylation, Catal. Today (2016), http://dx.doi.org/10.1016/j.cattod.2016.09.015

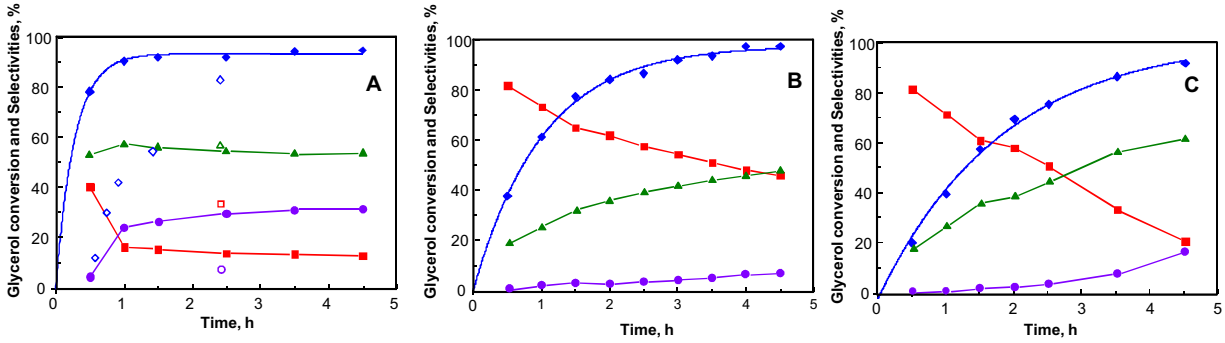

Fig. 8. Glycerol Conversion (♦) and selectivity to MAG (■), DAG (▲) and TAG (●) for samples Pr-SO_3H-SBA-15 (A), H-ZSM-5 (B) and H-Beta (C). Reuse results for Pr-SO_3H-SBA-15 sample are included in Fig. 8A, empty symbols.

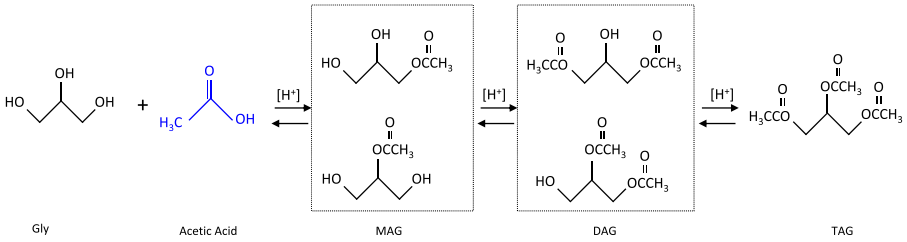

Scheme 1. Simplified reaction scheme for glycerol acetylation.

formation of the bulky TAG. Therefore, working on the synthesis is possible to accomplish a good number of acid sites with a correct distribution on the surface support. In addition, the pore size of the catalyst in this work was 3.2 nm, much lower than the 9.4 nm reported by Testa and coworkers. It is worth mentioning that the authors synthesized the catalyst performing the functionalization and oxidation in one step according to procedures described previously [48,56–58], whereas in this work the oxidation was made after the functionalization.

It is interesting to analyze the distribution of products at high reaction times for the studied zeolites. After 4.5 h reaction, the H-ZSM-5 has the highest amount of MAG (40%), similar to the percentage of DAG, being therefore very low the production of TAG. The porous structure characteristic of the zeolite H-ZSM-5, a two-dimensional pore system linked by much smaller channels, possibly hinders the formation of branched molecules as DAG, and further TAG.

The H-Beta zeolite was less active; however, at the end of the reaction it leads to an overall selectivity (DAG + TAG) of 79%, much better than the 54% obtained with the H-ZSM-5. This could be due to its three-dimensional porous structure, with higher pore diameter, that facilitates the formation of larger molecules and its diffusion.

Activity and selectivity results obtained with the H-ZSM-5 zeolite are similar to the results reported by Goncalves et al., [1], who also attributed the bad catalytic performance of this catalyst to diffusional problems.

The initial turnover frequencies were calculated using the initial reaction rates, obtained from the data reported in Fig. 7, and the acid sites concentration reported in Table 1. The TOF values resulted to be 16.2 s^{-1}, 6.75 s^{-1} and 3.01 s^{-1} for the Pr-SO_3H-SBA-15, H-ZSM-5 and H-Beta respectively. These results are presented in Fig. 9. It is very interesting to observe that the activity of each acid site is 2.4 times higher in the mesoporous catalyst as compared to the H-ZSM-5, and the latter is 2.2 times higher than in the case of the H-Beta zeolite, having both of them similar acid site density. Nevertheless, according to the TOF values, the strength of the acid

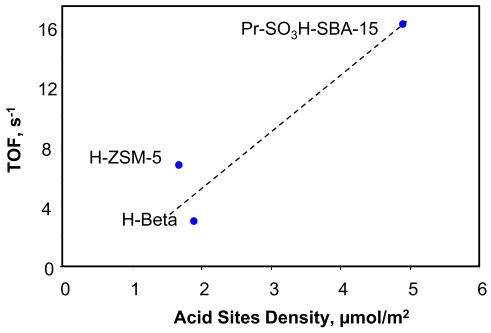

Fig. 9. Initial turn-over frequencies for glycerol conversion as a function of the acid sites density.

sites plays a major role in their intrinsic activity for the glycerol acetylation. The electrical potential determined for these catalysts suspended in acetonitrile was 724 mV, 480 mV, and 495 mV for Pr-SO_3H-SBA-15, H-ZSM-5 and H-Beta, respectively. Although it is not a conclusive evidence, these potentials are related to the strength of the acid sites. These results suggest that this parameter also plays a major role in defining the activity for the glycerol acetylation, as also suggested by other authors [21,29,30]. Clearly, the functionalized SBA-15 was the best catalyst among the studied materials. This catalyst has the higher acid site density and the higher strength of acid sites. Consequently, the activity as indicated by the TOF numbers was significantly higher than in the other two catalysts.

The initial electrical potentials obtained in the potentiometric titration experiments were similar for the two zeolites. Although it is indicative of the acid strength, it is not conclusive evidence in order to compare the two zeolites. On the other hand, the pyridine TPD results clearly shows that both zeolites have similar acid sites density but the strength is higher for the H-ZSM-5 material, and because of this, it has better activity. Furthermore, the H-ZSM-5 has an external surface higher than the H-Beta (see Table 1), which

Please cite this article in press as: B.O. Dalla Costa, et al., Influence of acidic properties of different solid acid catalysts for glycerol acetylation, Catal. Today (2016), http://dx.doi.org/10.1016/j.cattod.2016.09.015

can contribute to the improvement of the activity and stability. Kim et al. [21] obtained lower TOF with a Pr-SO_3H-SBA-15 that had lower acid site density than the catalyst used in the present study, although the higher temperature used by these authors was 100 °C, which is lower than the reaction temperature used in this work.

3.1.7. Pr-SO_3H-SBA-15 catalyst stability

The stability of the Pr-SO_3H-SBA-15 catalyst was studied conducting a second batch reaction under the same reaction conditions. Results are shown in Fig. 8A (open symbols). It can be observed that at 2.5 h the conversion was the same as 0.5 h in the first cycle, maintaining the distribution of products observed with the fresh material. Hence, it can be concluded that the catalyst suffers nonselective deactivation of acid sites. A possible cause of the deactivation could be the loss of functional groups by hydrolysis. In the presence of water, which is a byproduct of the reaction, these sulfonic acid groups could be removed from de surface as H_2SO_4. However, this was not previously observed for catalysts prepared by the co-condensation method [21]. Instead, this phenomenon was observed when the sulfonic acid group was grafted onto the support by a single ether type atomic linkage, using chlorosulfonic acid as a precursor [21]. Also, Testa el al. [29] employing XPS after the reaction ruled out the presence of leaching in the Pr-SO_3H-SBA-15 catalyst. In this work, the sulfur content of the solid catalyst was determined before and after the two reaction cycles by XRF. There was a decrease in the amount of sulfur of 10% relative to the fresh catalyst. This means that the number of active sites decreased proportionally, i.e. the acid site density was 10% lower in the catalyst used in the second cycle. This change does not seem enough to justify the important decrease in activity found in the second cycle. Therefore, we can infer that the deactivation is predominantly due to coke or reaction residues deposition on the active sites. This issue needs to be further investigated, since it is relevant regarding a possible application of this catalyst in large scale.

4. Conclusions

The glycerol acetylation was studied using different solid acid catalysts, two microporous zeolites (H-ZSM-5 and H-Beta), and a mesoporous material (SBA-15 functionalized with propylsulfonic groups). The Pr-SO_3H-SBA-15 catalyst presented the best performance, with a higher conversion (96%) and selectivity to DAG and TAG (87%) in 2.5 h reaction. This is achieved due to a proper balance between the amount of acid sites and their distribution on the surface, added to the mesoporous structure that facilitates the formation of bulky molecules.

This catalyst does not maintain the activity in consecutive cycles without treatment in between, although it but can be reused with acceptable results.

Among the zeolites, the best activity of H-ZSM-5 was associated to the strength of the acid sites. However, the selectivity to TAG was lower in this material, due to diffusive problems in the porous structure.

Acknowledgements

The authors acknowledge the financial support received from ANPCyT (PICT 2013, N°1252), UNL (PACT 69) and CONICET (PIO YPF-CONICET, 2013). Thanks are also given to ANPCyT for the purchase of the SPECS multitechnique analysis instrument (PME8-2003), and to Lic. M. Fernanda Mori for her technical assistance with the XPS equipment.

References

[1] V.L.C. Gonçalves, B.P. Pinto, J.C. Silva, C.J.A. Mota, Catal. Today 133 (2008) 673–677.
[2] M.Y. Huang, X.X. Han, C.T. Hung, J.C. Lin, P.H. Wu, J.C. Wu, S.B. Liu, J. Catal. 320 (2014) 42–51.
[3] X.M. Liu, H.Y. Ma, Y. Wu, C. Wang, M.A. Yang, P.F. Yan, U. Welz-Biermann, Green Chem. 13 (2011) 697–701.
[4] J.A. Sanchez, D.L. Hernandez, J.A. Moreno, F. Mondragon, J.J. Fernandez, Appl. Catal. A Gen. 405 (2011) 55–60.
[5] M.S. Khayoon, B.H. Hameed, Appl. Catal. A Gen. 433 (2012) 152–161.
[6] W. Isahak, Z.A.C. Ramli, M. Ismail, M.A. Yarmo, Ind. Eng. Chem. Res. 53 (2014) 10285–10293.
[7] L. Molinero, M. Ladero, J.J. Tamayo, F. Garcia-Ochoa, Chem. Eng. J. 247 (2014) 174–182.
[8] K. Jagadeeswaraiah, M. Prasad, P.S. Sai Prasad, N. Lingaiah, Appl. Catal. A Gen. 386 (2010) 166–170.
[9] M. Trejda, K. Stawicka, M. Ziolek, Appl. Catal. B Environ. 103 (2011) 404–412.
[10] S.H. Zhu, Y.L. Zhu, X.Q. Gao, T. Mao, Y.F. Zhu, Y.W. Li, Bioresour. Technol. 130 (2013) 45–51.
[11] P.S. Reddy, P. Sudarsanam, G. Raju, B.M. Reddy, Catal. Commun. 11 (2010) 1224–1228.
[12] A. Casas, J.R. Ruiz, M.J. Ramos, A. Perez, Energy Fuels 24 (2010) 4481–4489.
[13] J.A. Sanchez, D.L. Hernandez, J.A. Moreno, F. Mondragon, J.J. Fernandez, Appl. Catal. A Gen. 405 (2011) 55–60.
[14] P. Ferreira, I.M. Fonseca, A.M.J. Vital, J.E. Castanheiro, Catal. Commun. 10 (2009) 481–484.
[15] X. Liao, Y. Zhu, S.G. Wang, Y. Li, Fuel Process. Technol. 90 (2009) 988–993.
[16] X. Liao, Y. Zhu, S.-G. Wang, H. Chen, Y. Li, Appl. Catal. B Environ. 94 (2010) 64–70.
[17] L.N. Silva, V.L.C. Gonçalves, C.J.A. Mota, Catal. Commun. 11 (2010) 1036–1039.
[18] S. Kale, S.B. Umbarkar, M.K. Dongare, R. Eckelt, U. Armbruster, A. Martin, Appl. Catal. A Gen. 490 (2015) 10–16.
[19] I. Dosuna-Rodriguez, E.M. Gaigneaux, Catal. Today 195 (2012) 14–21.
[20] S. Bagheri, N.M. Julkapli, W.A. Yehye, Renew. Sust. Energy Rev. 41 (2015) 113–127.
[21] I. Kim, J. Kim, D. Lee, Appl. Catal. B Environ. 148–149 (2014) 295–303.
[22] J. Sun, X. Tong, L. Yu, J. Wan, Catal. Today 264 (2016) 115–122.
[23] S. Sandesh, P. Manjunathan, A.B. Halgeri, G.V. Shanbhag, RSC Adv. 5 (2015) 104354–104362.
[24] E.I. Basaldella, M.S. Legnoverde, I. Jiménez-Morales, E. Rodríguez-Castellón, B.O. Dalla Costa, C.A. Querini, Adsorption 17 (2011) 631.
[25] I.K. Mbaraka, D.R. Radu, V.S.Y. Lin, B.H. Shanks, J. Catal. 219 (2003) 329.
[26] S.Y. Chen, T. Yokoi, C.Y. Tang, L.Y. Jang, T. Tatsumi, J.C.C. Chan, S. Cheng, Green Chem. 13 (2011) 2920.
[27] A.F. Lee, J.A. Bennett, J.C. Manayil, K. Wilson, Chem. Soc. Rev. 43 (2014) 7887–7916.
[28] F. Zhou, J. Tang, Z. Fei, X. Zhou, X. Chen, M. Cui, X. Qiao, J. Porous Mater. 21 (2014) 149.
[29] M.L. Testa, V. La Parola, L.F. Liotta, A.M. Venezia, J. Mol, Catal. A: Chem. 367 (2013) 69–76.
[30] J.A. Melero, R. van Grieken, G. Morales, M. Paniagua, Energy Fuels 21 (2007) 1782–1791.
[31] W.D. Bossaert, D.E. DeVos, W.M. VanRhijn, J. Bullen, P.J. Grobet, P.A. Jacobs, J. Catal. 182 (1999) 156–164.
[32] D. Zhao, Q. Huo, J. Feng, B.H. Chmelka, G.D. Stucky, J. Am. Chem. Soc. 120 (1998) 6024–6036.
[33] S. Brunauer, P.H. Emmet, E. Teller, J. Am. Chem. Soc. 60 (1938) 309–319.
[34] B.C. Lippens, J.H. de Boer, J. Catal. 4 (1965) 319–323.
[35] E.P. Barrett, L.G. Joyner, P.P. Halenda, J. Am. Chem. Soc. 73 (1951) 373–380.
[36] M.L. Pisarello, B.O. Dalla Costa, N.S. Veizaga, C.A. Querini, Ind. Eng. Chem. Res. 49 (2010) 8935–8941.
[37] K.S.W. Sing, D.H. Everett, R.A.W. Haul, L. Moscou, R.A. Pierotti, J. Rouquerol, T. Siemieniewska, Pure Appl. Chem. 57 (1985) 603–619.
[38] S. Lowell, J.E. Shields, M.A. Thomas, M. Thommes, Characterization of Porous Solids and Powders: Surface Area, Pore Size and Density, Kluwer Academic Publishers, 2003.
[39] L. Sarkisov, P.A. Monson, Langmuir 17 (2001) 7600–7604.
[40] Chia-Hung Lee, Tien-Sung Lin, Chung-Yuan Mou, Nano Today 4 (2009) 165–179.
[41] S. Ruthstein, J. Schmidt, E. Kesselman, Y. Talmon, D. Goldfarb, J. Am, Chem. Soc. 128 (2006) 3366–3374.
[42] A.J. Crisci, M.H. Tucker, M.-Y. Lee, S.G. Jang, J.A. Dumesic, S.L. Scott, ACS Catal. 1 (2011) 719–728.
[43] I. Izquierdo-Barba, M. Colilla, M. Manzano, M. Vallet-Regí, Microporous Mesoporous Mater. 132 (2010) 442–452.
[44] G. Sartori, F. Bigi, R. Maggi, R. Sartorio, D.J. Macquarrie, M. Lenarda, L. Storaro, S. Coluccia, G. Martra, J. Catal. 222 (2004) 410–418.
[45] B. Stuart, Infrared Spectroscopy: Fundamentals and Applications, Wiley, New York, 2004.
[46] K. Grzechnik, K. Rutkowski, Z. Mielke, J. Mol. Struct. 1009 (2012) 96–102.
[47] J.P. Lourenço, M.I. Macedo, A. Fernandes, Catal. Commun. 19 (2012) 105–109.
[48] D. Margolese, J.A. Melero, S.C. Christiansen, B.F. Chmelka, G.D. Stucky, Chem. Mater. 12 (2000) 2448–2459.
[49] X. Shi, Y. Wu, H. Yi, G. Rui, P. Li, M. Yang, G. Wang, Energies 4 (2011) 669–684.

Please cite this article in press as: B.O. Dalla Costa, et al., Influence of acidic properties of different solid acid catalysts for glycerol acetylation, Catal. Today (2016), http://dx.doi.org/10.1016/j.cattod.2016.09.015

[50] M. Balaraju, P. Nikhitha, K. Jagadeeswaraih, K. Srilatha, P.S. Said Prasad, N. Lingaiah, Fuel Process. Technol. 91 (2010) 249–253.
[51] C.E. Gonçalves, L.O. Laier, A.L. Cardoso, M.J. da Silva, Fuel Process. Technol. 102 (2012) 46–52.
[52] X. Liao, Y. Zhu, S.G. Wang, H. Chen, Y. Li, Appl. Catal. B Environ. 94 (2010) 64–70.
[53] J.A. Melero, G. Vicente, G. Morales, M. Paniagua, J. Bustamante, Fuel 89 (2010) 2011–2018.
[54] E. García, M. Laca, E. Perez, A. Garrido, J. Peinado, Energy Fuels 22 (2008) 4274–4280.
[55] R. Wessendorf, Derivates of Glycerol as Components of Fuels, vol. 48, Erdol. Kohle, Erdgas, Pet., (1995), pp. 138–143.
[56] M. Choi, W. Heo, F. Kleitz, R. Ryoo, Chem. Commun (2003) 1340–1341.
[57] I.K. Mbaraka, B.H. Shanks, J. Catal. 229 (2005) 365–373.
[58] R. van Grieken, J.A. Melero, G. Morales, Appl. Catal. A Gen. 289 (2005) 143–152.

Please cite this article in press as: B.O. Dalla Costa, et al., Influence of acidic properties of different solid acid catalysts for glycerol acetylation, Catal. Today (2016), http://dx.doi.org/10.1016/j.cattod.2016.09.015